

A hybrid approach to machine learning annotation of large galaxy image databases

Evan Kuminski and Lior Shamir*

*Lawrence Technological University
21000 W Ten Mile Rd., Southfield, MI 48075
email: lshamir@mtu.edu

Abstract

Modern astronomy relies on massive databases collected by robotic telescopes and digital sky surveys, acquiring data in a much faster pace than what manual analysis can support. Among other data, these sky surveys collect information about millions and sometimes billions of extra-galactic objects. Since the very large number of objects makes manual observation impractical, automatic methods that can analyze and annotate extra-galactic objects are required to fully utilize the discovery power of these databases. Machine learning methods for annotation of celestial objects can be separated broadly into methods that use the photometric information collected by digital sky surveys, and methods that analyze the image of the object. Here we describe a hybrid method that combines photometry and image data to annotate galaxies by their morphology, and a method that uses that information to identify objects that are visually similar to a query object (query-by-example). The results are compared to using just photometric information from SDSS, and to using just the morphological descriptors extracted directly from the images. The comparison shows that for automatic classification the image data provide marginal addition to the information provided by the photometry data. For query-by-example, however, the analysis of the image data provides more information that improves the automatic detection substantially. The source code and binaries of the method can be downloaded through the Astrophysics Source Code Library.

Keywords: Image analysis, galaxies, galaxy morphology, pattern recognition,

machine learning, query-by-example.

1. Introduction

Modern astronomy has been becoming dependent on data obtained from autonomous digital sky surveys, allowing data-driven and statistical analysis that would not have been possible with manually controlled telescopes (Borne, 2013; Djorgovski et al., 2013; Edwards and Gaber, 2014). As the scales of these databases and the breadth of astronomical pipelines continue to grow, it is expected that efficient and reliable methods for analyzing these data will become crucial for astronomy research.

Perhaps the most basic method of annotating galaxies is through manual analysis performed by scientists (Arp and Madore, 1987; De Vaucouleurs et al., 1992; Nair and Abraham, 2010; Calvi et al., 2011; Baillard et al., 2011). Clearly, the main downside of that paradigm is its inability to handle the very large databases generated by modern digital sky surveys. To increase the bandwidth of manual annotation, crowdsourcing was used to allow non-expert volunteers to annotate galaxies through a web-based user interface (Lintott et al., 2011; Willett et al., 2013). However, despite the ability of non-experts to provide useful information about galaxies, the rapidly growing size of these databases makes them far too massive for even a relatively large group of volunteers.

Previously proposed automatic methods for galaxy annotation are based on the application of image processing and computer vision techniques (Abraham et al., 2003; Lekshmi et al., 2003; Peng et al., 2011; Simard, 1998; Baillard et al., 2006; Shamir, 2009, 2011b; Kuminski et al., 2014; Dieleman et al., 2015; Schutter and Shamir, 2015; Shamir et al., 2013a; Davis and Hayes, 2014; Hocking et al., 2017), and the application of these algorithms to databases collected by digital sky surveys produced catalogs of morphological information (Huertas-Company et al., 2010, 2016; Shamir and Wallin, 2014; Kuminski and Shamir, 2016; Timmis and Shamir, 2017). These catalogs demonstrate that automatic analysis of galaxy images is a practical solution to the problem of annotating

large databases of astronomical images.

Another approach to automatic classification and annotation of galaxies is by analyzing the spectroscopic or photometric information produced by the digital sky survey (Ball et al., 2004, 2006; Almeida et al., 2010; Banerji et al., 2010; Vasconcellos et al., 2011). That approach does not require direct analysis of the image, but instead the automatic classifier can use a combination of measurements collected by the photometric pipeline of the digital sky survey. The digital sky survey pipelines can provide information that cannot be obtained from the image alone, such as the magnitude of the object in the different bands. However, the information provided by the pipeline is limited to a set of pre-defined measurements that do not contain all information about the galaxy morphology, and full reconstruction of the galaxy morphology using these measurements alone is normally not possible.

Here we combine the analysis of photometric data and computer vision to propose a hybrid method that classifies and detects celestial objects based on both image and photometry data collected by sky surveys. The method combines the pre-defined commonly used photometric measurements with features extracted directly from the images to measure and compare the amount of information that the direct analysis of the images can add to the photometric measurements. Since many modern sky surveys such as Sloan Digital Sky Survey (SDSS) or the Panoramic Survey Telescope and Rapid Response System (PanSTARRS) provide both photometry and image data, such method can be used to perform automatic tasks related to the annotation of celestial objects in large astronomical databases.

2. Data

Data were used for two different experiments. The first set of experiments is automatic annotation of galaxy images. That is, given a galaxy image the algorithm annotates the galaxy based on its morphology, and classify visual elements such as the spirality, bulge, number of arms, etc (Willett et al., 2013;

Kuminski et al., 2014; Dieleman et al., 2015).

The second set of experiments is query-by-example (Shamir, 2016). Query-by-example allows a researcher to provide the system with a sample of a certain galaxy of interest, and the system returns a list of objects that are the most similar to the query object, allowing the studying of that object using more than one galaxy of the same type. Clearly, the availability of a group of similar objects allows statistical analysis of their characteristics, such that $N > 1$.

2.1. Data for the automatic annotation of galaxies

The data used in the experiment are taken from SDSS, and annotated by Galaxy Zoo 2 (Willett et al., 2013), as thoroughly explained in (Kuminski et al., 2014). The images are JPEG images of dimensionality of 120×120 pixels, downloaded through SDSS’s Catalog Archive Server (CAS). The JPEG images are generated in the CAS database by combining the FITS images taken in the i, r, and g bands, invoked in each request sent to the ImgCutout service of CAS (Lupton et al., 2004). The images are generated after applying de-noising and several filters that can change the images, and ignores the b and z bands, and therefore the JPEG images might not contain all information contained in the raw FITS images. However, these JPEG images normally contain complete information that allows to visually determine the morphology of the galaxy, and therefore these images are the most informative images to be used by machine learning systems compared to using the individual bands.

The galaxies in the Galaxy Zoo 2 catalog have different angular sizes, so the galaxy images are downloaded in an iterative process starting with a scale of 0.1” per pixel. The image is separated to foreground and background pixels using the Otsu binary transform (Otsu, 1979), and the scale is increased by 0.05” per pixel until no more than 40 foreground pixels are located on the edge of the frame. The iterative scaling of the images ensures that the object fits inside the frame.

The data used in this study are the original 245,609 Galaxy Zoo 2 images, and the morphological annotations associated with each image. Since each

galaxy is annotated by 44 non-expert participants on average, the resulting annotation of each galaxy and each question is determined statistically by the distribution of the votes. Naturally, when the level of agreement between the voter gets higher, the annotation can be considered more likely to be correct (Lintott et al., 2011).

The distribution of the votes for each question provided the ground truth data for the experiments. To reduce possible noise, only questions that their answers in the context of a certain galaxy reached a certain threshold of agreement were used. When the distribution of the answers for a certain galaxy does not reach that threshold, the galaxy is rejected and not used in the experiment. A detailed description of the data can be found in (Kuminski et al., 2014).

The size of the dataset for each question changes with the agreement threshold. The sizes of the classes and the total size of the dataset of each question are specified in (Kuminski et al., 2014), and also in Table 1. To avoid bias due to differences in the sizes of the classes in the GZ2 sample, the size of each class equals to the number of galaxies in the smallest class (Kuminski et al., 2014).

2.2. Data for galaxy query-by-example experiments

The set of galaxies used in the query-by-example experiments is described in (Shamir, 2016). That data is also taken from SDSS, downloaded in the same manner, and provided several datasets. The first dataset contains galaxies classified into spiral or elliptical galaxies (Kuminski and Shamir, 2016). In a universe that contains just early-type galaxies, a spiral galaxy would be considered “peculiar”, and therefore a small set of spiral galaxies can be combined with a larger number of elliptical galaxies, and then each of the spiral galaxy images can be used as a query galaxy. The performance can be measured by the number of spiral galaxies among the total number of galaxies returned by the queries.

The first dataset contains 100 spiral galaxies and 100 elliptical galaxies taken from (Kuminski and Shamir, 2016). The galaxies were visually inspected, and used also in (Shamir, 2016). The elliptical and spiral galaxies were also combined

Question	>50%	>60%	>70%	>80%	>90%	>95%	>97%
1	25000 (241679)	25000 (213890)	25000 (181715)	25000 (132748)	19693 (50946)	6635 (19248)	2332 (12193)
2	10367 (61515)	6705 (53058)	3955 (41193)	2003 (27891)	645 (18325)	225 (10154)	127 (6761)
3	13993 (55488)	9964 (46176)	6506 (37181)	3720 (27788)	1399 (17646)	386 (9913)	171 (6629)
4	9846 (55396)	4334 (42130)	1522 (32119)	323 (23681)	11 (15106)	1 (8421)	0 (5479)
5	13028 (42780)	5866 (24385)	510 (10583)	110 (2499)	3 (143)	0 (9)	0 (2)
6	22889 (242291)	15791 (224645)	9921 (202509)	5369 (170574)	1957 (115692)	691 (65638)	417 (46159)
7	24203 (172761)	16442 (138128)	8593 (100328)	2117 (55774)	103 (9545)	6 (961)	4 (221)
8	37 (15219)	9 (7483)	1 (3078)	0 (1008)	0 (163)	0 (18)	0 (11)
9	97 (9272)	44 (4860)	18 (2076)	8 (562)	3 (48)	0 (4)	0 (1)
10	5471 (33536)	3371 (16289)	1337 (6332)	119 (2061)	6 (469)	0 (118)	0 (51)
11	226 (21814)	120 (14966)	58 (10900)	24 (8490)	0 (5948)	0 (3568)	0 (2343)

Table 1: The size of each class used for automatic annotation and the total number of galaxies (in parentheses) for each GZ2 agreement threshold (Kuminski et al., 2014).

with 20 ring galaxies and 20 galaxy pairs (Shamir, 2016) as the query galaxies.

In addition to the smaller datasets, another dataset of 4,000 images of galaxies classified as spiral and 4,000 images of galaxies classified as elliptical were used in combination with ring and galaxy pairs. These elliptical and spiral galaxies are also taken from the catalog of SDSS galaxies classified by their broad morphology (Kuminski and Shamir, 2016).

3. Methods

3.1. Morphological features

The morphological features used in this experiment are based on the morphological features of the Wndchrm scheme (Shamir et al., 2008, 2013b), which demonstrated its ability to analyze galaxy images (Shamir, 2009; Shamir et al.,

2013a; Kuminski et al., 2014). The method works by first extracting a large set of numerical image content descriptors, including texture features such as the Tamura, Gabor, and Haralick textures, pixel intensity distribution such as multi-scale histograms and first four moments, shape features such as edge and object statistics, polynomial decomposition such as Chebyshev statistics and Zernike polynomial, Radon features, fractals, and the Gini coefficient (Abraham et al., 2003). One of the unique elements of Wndchrm is that the numerical image content descriptors are computed not just from the original image, but also from transforms of the image. The transforms used by the algorithm are the Fourier transform, Chebyshev transform, Wavelet transform (Symlet 5), and edge magnitude transform, in addition to combinations of these transforms. These morphological features were used for both the automatic annotation and the query-by-example experiments. A detailed description of the numerical image content descriptors can be found in (Shamir et al., 2008; Shamir, 2009; Shamir et al., 2013a, 2009, 2014), and the source code is publicly available (Shamir et al., 2013b).

3.2. Photometric features

Photometric data were obtained from SDSS Data Release 7 (Abazajian et al., 2009), and included the 453 columns of the PhotoObjAll table. To avoid incomplete data, objects that had missing or bad measurement values of -1000 or -9999 were rejected from the experiment, reducing the Galaxy Zoo 2 dataset to 138,232 objects with complete photometric values in the PhotoObjAll table. These features are added to the morphological features to create a single feature vector that contains both morphological and photometric features. For instance, the 453 photometric features are added to the 2,883 morphological features to create a feature vector of the size of 3,336 features.

While not all fields in the PhotoObjAll table are necessarily informative (e.g., the object ID), the use of feature selection as will be described in Section 3.3.1 automatically removes features that do not provide meaningful information.

3.3. Pattern recognition

3.3.1. Classification

The classification is based on the Weighted Nearest Distance (WND) scheme (Orlov et al., 2008; Shamir et al., 2008). First, all morphological and photometric features are normalized to the interval $[0,1]$, and assigned with Fisher discriminants scores (Bishop, 2006). The 85% of the features with the lowest Fisher discriminant scores are rejected, and the remaining features are used by the Weighted Nearest Distance (WND) classifier such that the Fisher discriminant scores are used as weights (Orlov et al., 2008; Shamir et al., 2008).

The WND classifier is based on the distance shown in Equation 1

$$d(x, c) = \frac{\sum_{t \in T_c} [\sum_{f=1}^{|x|} W_f^2 (x_f - t_f)^2]^p}{|T_c|} \quad (1)$$

where T is the entire training set, T_c is the training set of class c , t is a feature vector from T_c , x is the feature vector of the galaxy image being classified, $|x|$ is the size of feature vector, x_f is the value of image feature f , W_f is the Fisher discriminant score of feature f , $|T_c|$ is the number of training samples of class c , $d(x, c)$ is the computed distance from a given sample x to class c , and p is the exponent, which is set to -5 as described in detail with empirical results in (Orlov et al., 2008). Naturally, the class c that has the shortest distance to the sample x is determined as the predicted class.

The performance is measured simply by the number of correct annotations made by the algorithm, divided by the total number of galaxies being annotated. An annotation is considered correct if the annotation made by the computer is the same as the annotation made by the majority of the Galaxy Zoo 2 citizen scientists. The “majority” threshold is dynamic, and different thresholds are tested for each question as will be described in Section 4.

3.3.2. Query by example

The pattern recognition for the query-by-example method is described in (Shamir, 2016). The method is based on the same numerical image content

descriptors mentioned in Sections 3.1 and 3.2, but measures the distances between the query object and each of the objects in the dataset using weighted Euclidean distance or by Earth Mover’s Distance (Rubner et al., 2000), after weighting the descriptors by their entropy (Shamir, 2016). The source code of the method is publicly available (Shamir, 2017). As shown in (Shamir, 2016), the best performance of the query-by-example algorithm is achieved when using entropy weights and Earth’s Movers Distances.

The performance of the query by example is measured by using two sets of galaxies – a database set and a query set. The database set contains galaxies that are the typical non-peculiar galaxies in the database, and the query set contains galaxies of interest that the algorithm attempts to find among the galaxies in the database set.

The performance evaluation is done by merging P galaxies from the query set with Q galaxies from the database set. Then, one of the galaxies from the query set is selected as the query galaxy, while a subset of the remaining $P-1$ galaxies is merged with the Q database galaxies, and the algorithm returns the R galaxies that the algorithm determines are the most similar to the query galaxy image. The process is repeated P times such that all galaxies in the query set are used once as the query galaxy.

The performance is determined by Equation 2

$$\frac{\sum_{p=1}^{|P|} \sum_{r=1}^{|R_p|} (R_{p_r} \in P \wedge R_{p_r} \neq p)}{|P|}, \quad (2)$$

where R_p is the set of galaxies returned by the algorithm as the most similar to the query galaxy image p .

The rank is defined as the size of the set R_p . If a galaxy from the query set P is present among the R galaxies the query is considered a hit. The performance is determined by the hit rate, which is the average number of galaxies of the query set P among the R galaxies returned by the method in each of the $|P|$ queries it attempts. That process is repeated iteratively such that in each run a different galaxy p is used as the query galaxy, and the performance is evaluated

by the average number of galaxies of the query set among the top R galaxies returned by the query.

The method is not expected to be fully accurate, and therefore it is expected that the set R returned by the method can also contain many galaxies that are not of the same type as the query galaxy. However, the purpose of the method is to reduce the data and provide a smaller dataset in which the frequency of galaxies similar to the query galaxy is much higher compared to their population in the database (Shamir, 2016).

4. Results

4.1. Classification

To quantify the efficacy of combining morphological data and photometric data, we ran a series of tests using the results of Galaxy Zoo 2 data described in Section 2 to obtain training and test data. By changing the threshold of agreement we controlled the trade-off between the size of the training set and the cleanness of the data. Setting a high threshold for the vote fraction leads to a smaller but cleaner dataset, as higher agreement rate between the voters leads to cleaner annotations. Lower threshold provides a larger dataset in which more objects are more likely to have been misclassified. This process is explained in greater detail in (Kuminski et al., 2014).

For each of the training sets that were generated, the algorithm was tested with the three feature sets described in Section 3: the photometric features, the morphological features, and a combination of both morphological and photometric feature sets. This was done to verify that the algorithm could draw useful information from the photometric data, and to then evaluate how the combined feature set is compared to the morphological and photometric feature sets.

As done in (Kuminski et al., 2014) and mentioned in Section 3, each question in GZ2 is tested by separating the data based on the degree of agreement among the citizen scientists who annotated that question. That was repeated

for each degree of agreement, so that only galaxies that were annotated with that agreement level or higher are used, and the rest of the galaxies are rejected from the experiment.

Figure 1 shows the automatic classification accuracy when the galaxies are separated into classes based on the manual annotations of the different questions in Galaxy Zoo 2. That is, the manual annotations of the galaxies obtained through the Galaxy Zoo 2 campaign are used as ground truth for training and testing the machine learning algorithm. When the Galaxy Zoo 2 agreement threshold of the annotation is increased, less galaxies are used for training. That can lead to a decrease in classification accuracy, as the performance of machine learning algorithms depends on the size of the training set. However, including galaxies on which the agreement between the citizen scientists is higher leads to a cleaner and more consistent dataset (Lintott et al., 2011), which can compensate for the smaller size of the training data.

As the graphs show, the classification accuracy for most questions using the photometric features was similar to the classification accuracy achieved using the morphological features, but in seven of the nine cases using the photometric features provided higher accuracy in comparison to the morphological features. When combining the photometric and morphological features, in most cases the classification accuracy is improved for the different questions and different threshold values compared to using either the photometric features or the morphological features alone. Perhaps the only notable exception is question 2 (“Could this be a disk viewed edge-on?”), in which the photometric features outperform the combined feature set when using galaxies that were annotated by the Galaxy Zoo 2 volunteers in agreement level of 90–95%. It should be noted that while the answer to that question is boolean (“yes” or “no”), there are many in-between cases based on the position of the galaxy in comparison to Earth. Question 8 (odd features) and 9 (bulge shape) of Galaxy Zoo 2 were not used due to the low number of sample classifications.

The algorithm selects the most informative features automatically based on their Fisher discriminant scores. The top 30 descriptors and their Fisher discrim-

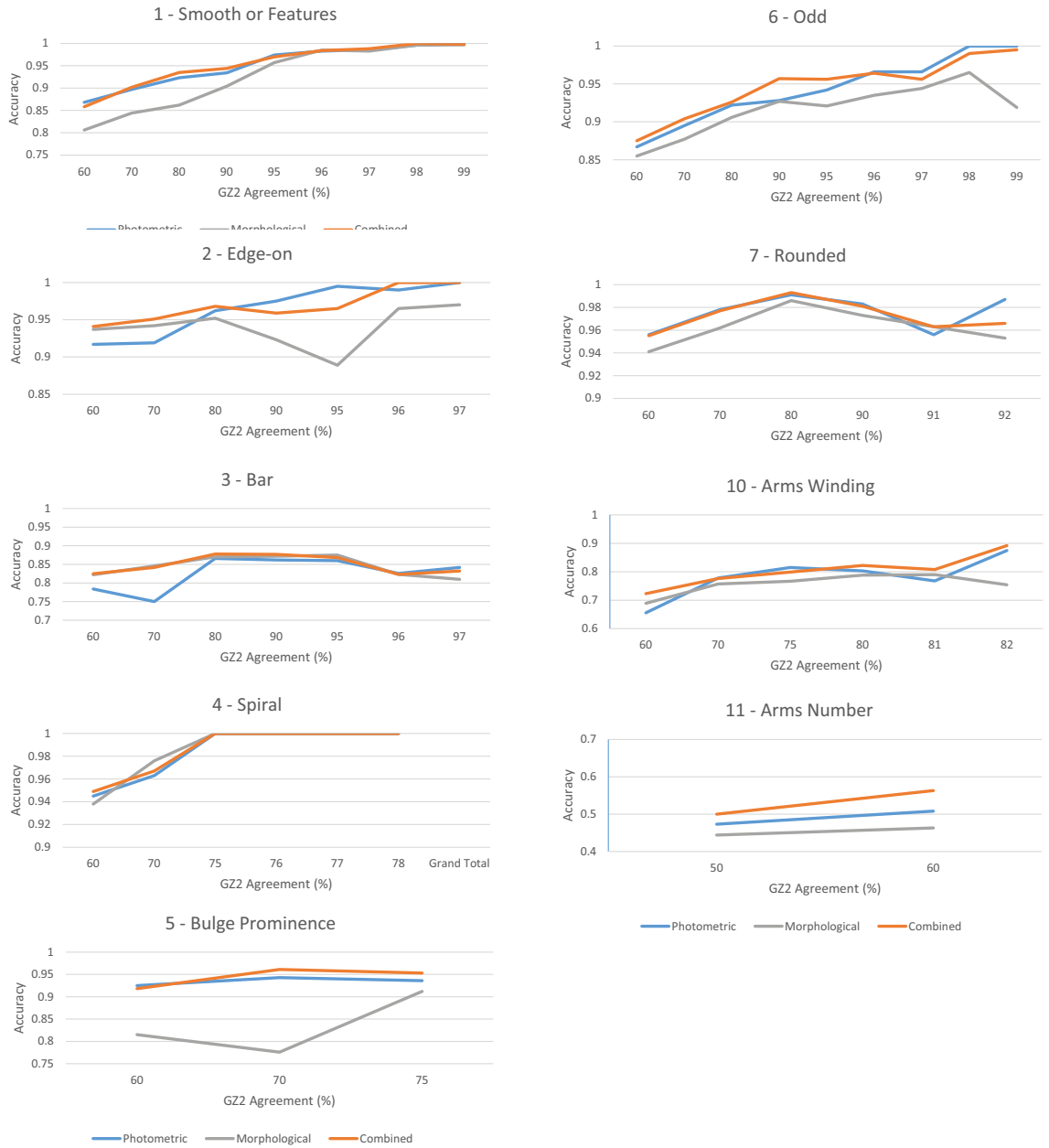


Figure 1: Comparison of the classification accuracy for different feature sets when applied to different question in Galaxy Zoo 2.

inant scores when using the morphological features, the photometric features, and the combined features used in Question 1 (whether the galaxy is round and smooth) are specified in Table 2 ranked by their Fisher discriminant scores. The most informative photometric feature in the context of Question 1 is rho (log size for surface brightness in the i band). Among the morphological features, most of the features were texture features (e.g, Haralick) and Fractals.

Rank	Morphological features	Photometric features	Combined feature set
1	Haarlick Texture 5 (Fourier Chebyshev) : 3.52	rho: 4.34	rho: 4.35
2	Fractal bin 3 (Chebyshev) : 3.194908	deVMag-u: 3.77	deVMag-u: 3.77
3	Haarlick Texture 10 (Fourier Wavelet) : 3.15	petroR50-u: 3.42	Haarlick Texture 5 (Fourier Chebyshev): 3.52
4	Haarlick Texture 0 (Fourier Wavelet) : 3.09	deVMag-g: 3.4	deVMag-g: 3.41
5	Haarlick Texture 18 (Fourier Wavelet) : 2.95	expRad-g: 3.31	petroR50-u: 3.38
6	Fractal bin 11 (Chebyshev Wavelet) : 2.91	petroR50-g: 3.31	expRad-g: 3.32
7	Haarlick Texture 20 (Fourier Wavelet) : 2.84	expMag-u: 3.3	expMag-u: 3.31
8	Fractal bin 6 (Chebyshev Wavelet) : 2.84	deVRad-u: 3.12	petroR50-g: 3.27
9	Haarlick Texture 8 (Fourier Wavelet) : 2.8	petroR50-r: 3.12	Fractal bin 3 (Chebyshev): 3.22
10	Fractal bin 10 (Chebyshev Wavelet) : 2.78	petroR50-i: 3.05	Haarlick Texture 10 (Fourier Wavelet): 3.19
11	Haarlick Texture 4 (Fourier Chebyshev) : 2.75	expRad-r: 3.02	Haarlick Texture 0 (Fourier Wavelet): 3.16
12	Haarlick Texture 14 (Fourier Wavelet) : 2.73	petroR50-z: 2.99	deVRad-u: 3.15
13	mean (Fourier Wavelet) : 2.726157	deVRad-g: 2.98	petroR50-r: 3.1
14	Fractal bin 5 (Chebyshev Wavelet) : 2.72	petroRad-g: 2.91	petroR50-i: 3.02
15	Haarlick Texture 12 (Fourier Wavelet) : 2.72	petroMag-u: 2.89	deVRad-g: 3
16	Fractal bin 15 (Chebyshev Wavelet) : 2.7	expRad-i: 2.89	expRad-r: 2.99
17	Fractal bin 4 (Chebyshev Wavelet) : 2.68	petroRad-r: 2.84	Haarlick Texture 18 (Fourier Wavelet): 2.99
18	MultiScale Histogram bin 1 (Wavelet) : 2.67	expRad-u: 2.83	petroR50-z: 2.97
19	Fractal bin 16 (Chebyshev Wavelet) : 2.67	dered-u: 2.81	Fractal bin 11 (Chebyshev Wavelet): 2.89
20	Zernike bin 2 () : 2.658163	expMag-g: 2.79	petroRad-g: 2.89
21	gini coefficient (Fourier Chebyshev) : 2.63	petroRad-i: 2.79	Haarlick Texture 20 (Fourier Wavelet): 2.89
22	Zernike bin 12 (Wavelet) : 2.630277	modelMag-u: 2.74	expRad-i: 2.89
23	Fractal bin 12 (Chebyshev Wavelet) : 2.63	modelMag-u: 2.74	petroMag-u: 2.89
24	Fractal bin 19 (Chebyshev Wavelet) : 2.62	deVMag-r: 2.56	expRad-u: 2.84
25	gini coefficient (Chebyshev Fourier) : 2.62	petroRad-u: 2.47	dered-u: 2.82
26	Fractal bin 14 (Chebyshev Wavelet) : 2.61	petroMag-g: 2.41	Fractal bin 6 (Chebyshev Wavelet): 2.82
27	Haarlick Texture 24 (Fourier Wavelet) : 2.61	deVRad-r: 2.41	Haarlick Texture 8 (Fourier Wavelet): 2.82
28	CombFirstFourMoments 11 (Wavelet) : 2.61	isoA-u: 2.4	petroRad-r: 2.81
29	Zernike bin 0 (Edge Transform) : 2.6	expRad-z: 2.40	expMag-g: 2.8
30	Fractal bin 7 (Chebyshev) : 2.58	petroRad-z: 2.38	petroRad-i: 2.79

Table 2: The most informative morphological and photometric features and their Fisher discriminant scores. These features are used for question 1, which is whether the galaxy is round and smooth.

The table shows that among the top 30 features in the combined feature set, 21 were photometric features. Among the 100 most informative features 34 were photometric features, while 66 were the morphological features. Figure 2 shows the amount of photometric and morphological features among the 30 and 100 most informative descriptors for each of the Galaxy Zoo 2 questions that

provided the ground truth information for the experiments. The figure shows that the most informative features can be mostly photometric or morphological based on the specific question.

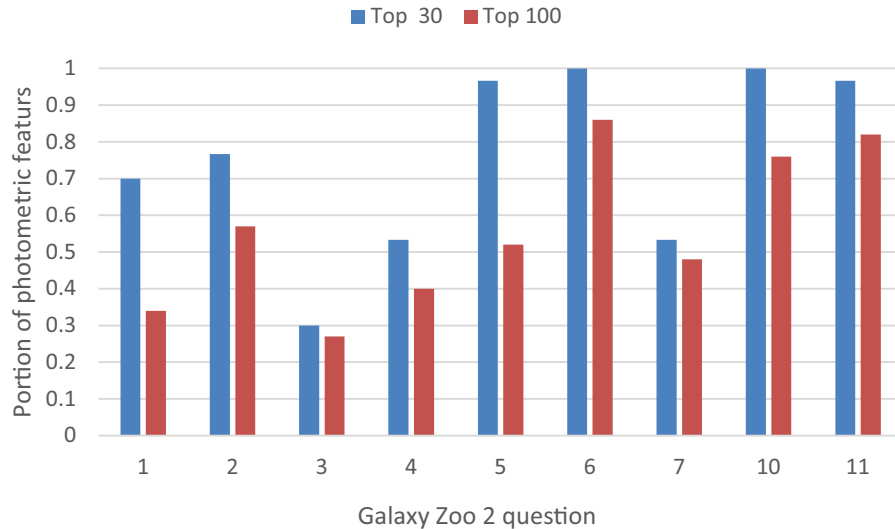


Figure 2: Portion of photometric features among the 30 and 100 most informative features for the analysis of the different Galaxy Zoo 2 questions.

As Table 2 shows, the photometric features that are assessed as the most informative and have the highest impact on the analysis are not features that reflect the morphology of the galaxy directly, but are related to size (e.g. Petrosian radius) and brightness (e.g., model magnitude). These features correlate with the different types of galaxies, and their combination provides patterns that allow the identification of the morphology of the galaxy without measuring it directly. On the other hand, the machine vision-based morphological features are features such as fractals and textures, that are clearly driven directly by the shape of the galaxy and reflect its the morphology.

Figure 3 shows examples of false positives and false negative classifications, such that the ground truth is the Galaxy Zoo 2 “superclean” classifications. These false detection show that galaxies identified as ellipticals by the method

can in fact be spiral galaxies. On the other hand, galaxies identified as elliptical by human annotators might sometimes have spiral features in them, as clearly seen in galaxy 587736915143229734. These differences between human and machine classification are aligned with the observation that human classifiers tend to misidentify spiral galaxies and annotate them as elliptical (Dojcsak and Shamir, 2014).

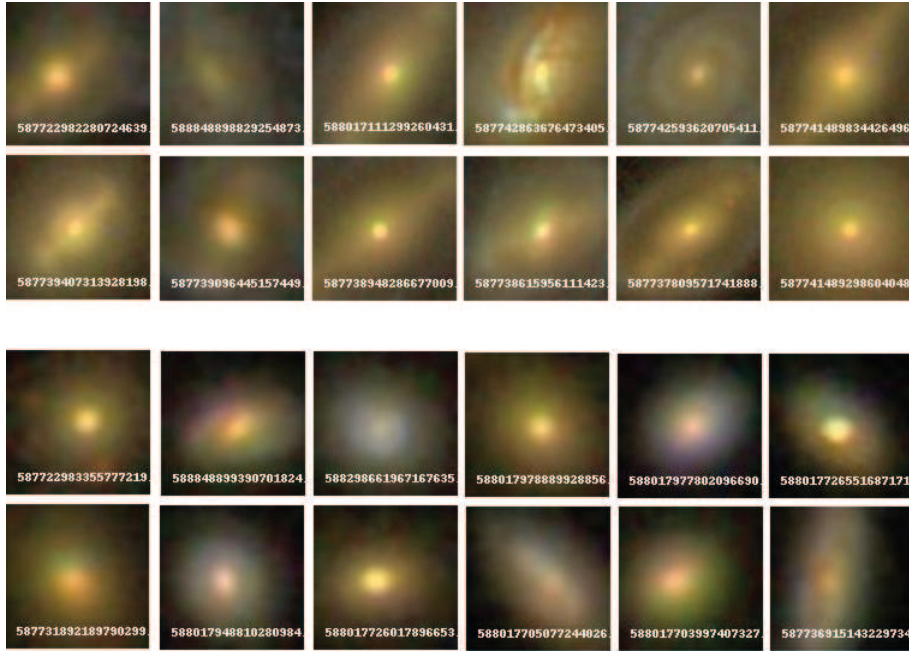


Figure 3: Examples of false detections of spiral and elliptical galaxies. The top two lines are galaxies that were classified by Galaxy Zoo 2 as “superclean” spiral but were classified by the method as elliptical, and the bottom line shows galaxies that were classified by Galaxy Zoo 2 as elliptical but the method identified them as spiral. The DR8 IDs were added to the images to allow the identification of the specific galaxies, but were not part of the original galaxy images.

4.2. Query by example

The hit rate when using the morphological features, photometric features, and combined feature sets are shown in Figures 4 through 10. Figure 4 shows the hit rate when using 100 spiral galaxies as the regular galaxies and 10 elliptical

galaxies as the peculiar galaxies. As explained in Section 3.3.2, the test is performed multiple times such that in each run different query images are used for testing. The test is performed 100 times such that 10 randomly selected elliptical galaxies are used as the “peculiar” galaxies, and one is selected as the query galaxy. The hit rate naturally changes based on the rank, as a larger number of galaxies returned by the query increases the chance that one of them is of the same type as the query galaxy. Similarly, Figure 5 shows the hit rate when attempting to return automatically the R most similar galaxies to a query spiral galaxy among a dataset of 110 galaxies – 100 elliptical galaxies and 10 spiral galaxies. In both cases the combined feature set that includes both the morphological and photometric features outperforms the performance when using the morphological or photometric features alone.

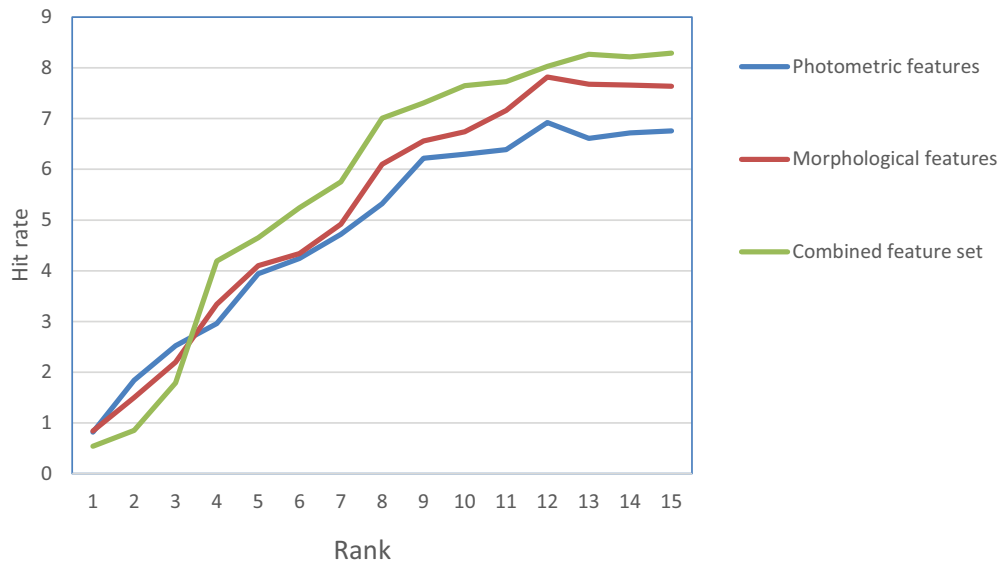


Figure 4: Hit rate of the query by example algorithm when using 100 spiral galaxies as the database class and 10 elliptical galaxies as the query galaxies. The experiment was repeated with the morphological features alone, the photometric features alone, and both photometric and morphological features.

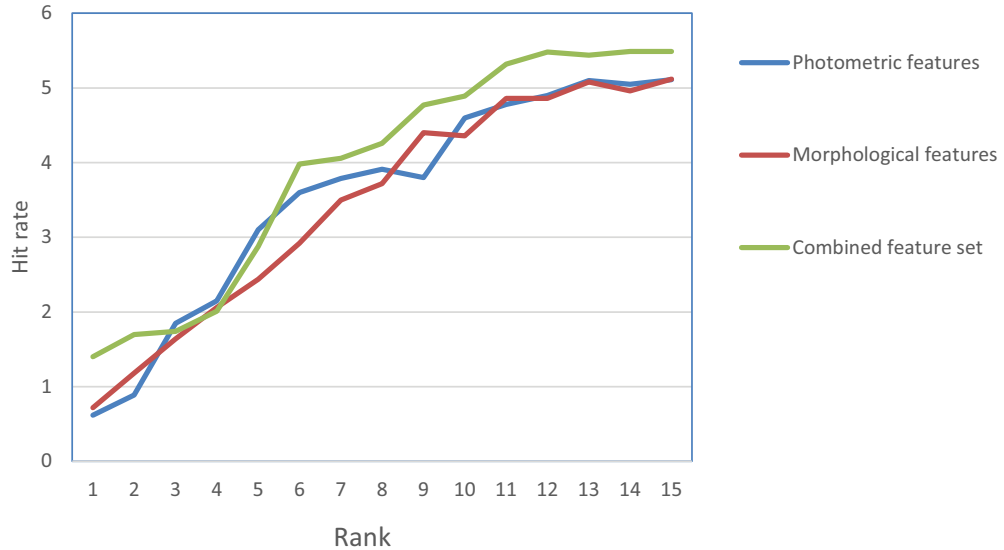


Figure 5: Hit rate of the query by example algorithm with the different feature sets when using 100 elliptical galaxies as the database class and 10 spiral galaxies as the query galaxies.

Another experiment attempted to identify ring galaxies based on a query image. The database galaxies in this experiment were 100 elliptical galaxies, and the query galaxies were 20 ring galaxies used in (Shamir, 2016). In each run a different ring galaxy is used as the query galaxy, and 10 ring galaxies are combined with the 100 images of elliptical galaxies. Similarly, an additional experiment used the same ring galaxies among 100 spiral galaxies. Figures 6 and 7 show the hit rate of the ring galaxies among the elliptical and spiral galaxies, respectively. In both cases using the combination of morphological and photometric features increased the number of ring galaxies returned by the algorithm given the query ring galaxy image.

To test actual peculiar systems, we combined a set of 20 tidally distorted galaxy pairs with 400 non-peculiar galaxy pairs taken from Sloan Digital Sky Survey. The peculiar galaxy pairs were taken from the catalog of automatically-identified galaxy pairs (Shamir and Wallin, 2014), and displayed by Figure 8.

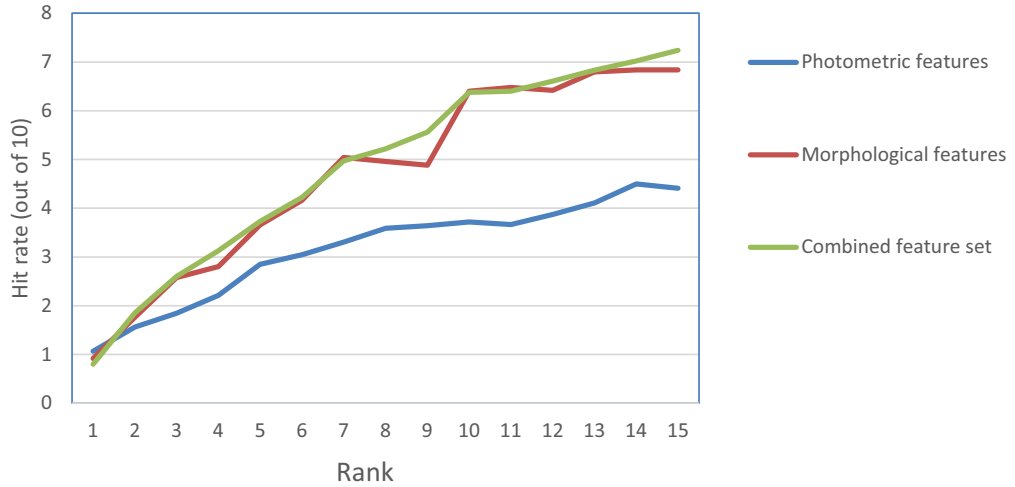


Figure 6: Hit rate of the query-by-example algorithm when 10 ring galaxies are combined with 100 elliptical galaxies. The algorithm is performed with the morphological features, the photometric features, and the combined feature set.

Figure 9 shows the average hit rate when using one peculiar galaxy pair as the query galaxy, such that each of the 20 galaxies is used as the query galaxy for each rank. The results show that the photometric features alone provide low hit rate compared to the morphological features and the combined feature sets.

To test the completeness of the query-by-example algorithm, 4,000 elliptical galaxies were combined with 1,000 spiral galaxies, and a spiral galaxy was used as the query image. A similar experiment was done with 4,000 spiral galaxies merged with 1,000 images of elliptical galaxies, and an elliptical galaxy used as the query image in each run. As before, the experiment was repeated such that in each run a different image was used as the query image. The fraction of the target galaxies in the database among the galaxies returned by the query is shown in Figure 10. As expected, the combined feature set provides more information, allowing the higher frequency of the target galaxies that are similar to the query galaxy.

Figure 11 shows the distribution of the photometric and morphological fea-

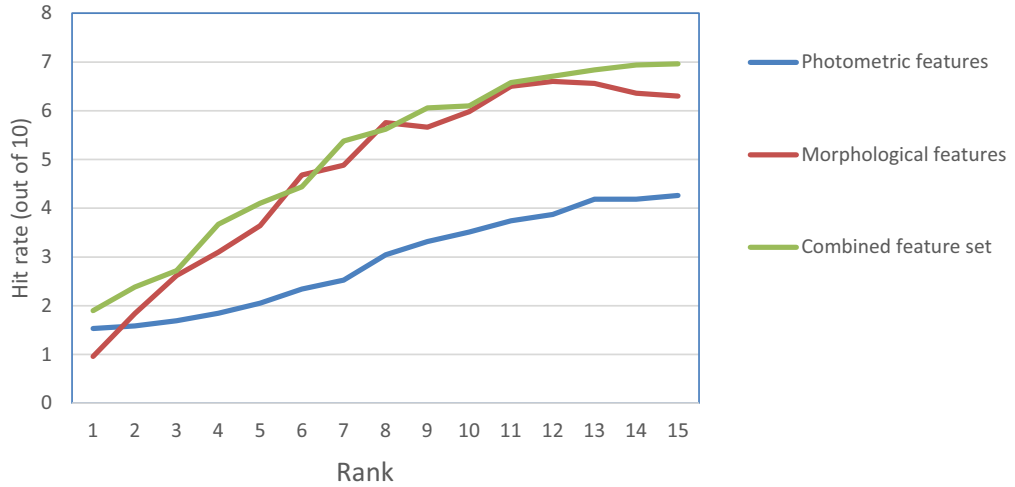


Figure 7: Hit rate of the query by example algorithm of the different feature set when using 100 spiral galaxies and 10 ring galaxies, and the query galaxy is a ring galaxy.

tures used for each of the experiments. These features are selected by their entropy as a heuristic estimation of their usefulness in identifying similar galaxies to a given query galaxy (Shamir, 2016). In each experiment different features can be selected based on the data, but the figure shows that in general more morphological features are ranked higher than the photometric measurements. However, the number of morphological features is also much higher than the number of photometric features (2898 compared to 418), so higher noise in the feature selection process is expected to lead to an increased representation of morphological features.

5. Correlation between photometry and morphology

The set of photometric variables collected by SDSS is clearly not orthogonal, and many of these variables correlate with each other. To test the correlation between the different individual photometric variables and the morphology of the galaxies we performed a regression between the images and each of the photometric variables, and measured the Pearson correlation between the values

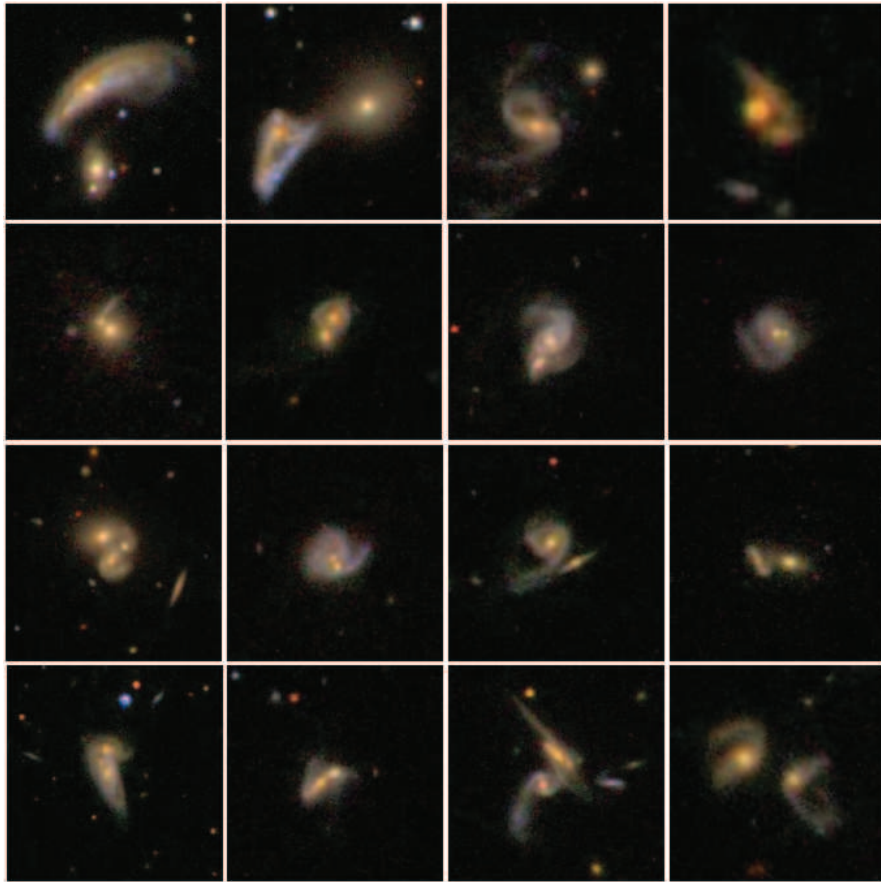


Figure 8: Tidally distorted galaxy pairs taken from the catalog of automatically detected peculiar galaxy pairs (Shamir and Wallin, 2014).

of each photometric variable and the morphology of the galaxy as measured by the morphological features described briefly in Section 3.1. That was done by attempting to predict the value of the variable by first training a machine learning system, and then using a test set to compare between the predicted value and the actual value of the variable, such that the value is predicted by using the galaxy image as the input. High correlation between the value predicted when the galaxy image is used as input and the actual value of the variable indicates a link between the variable and the morphology of the galaxies.

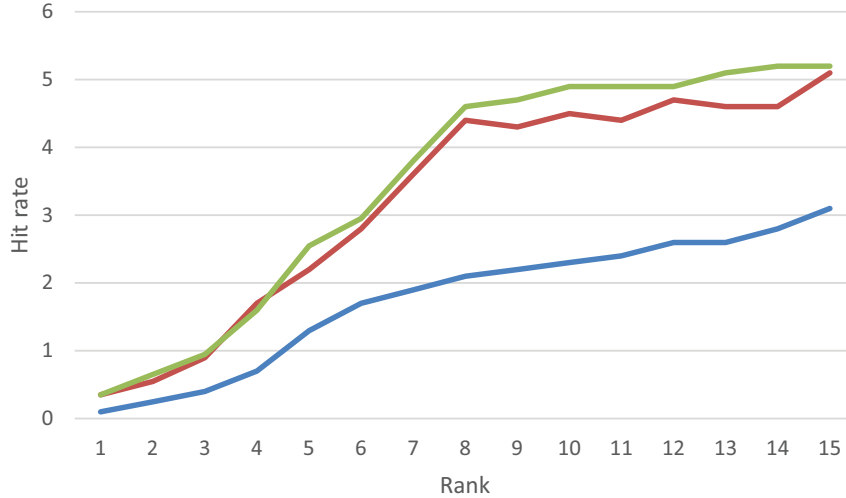


Figure 9: Hit rate of the query-by-example algorithm when retrieving 20 peculiar galaxy pairs among 400 galaxies, and the query galaxy is a galaxy pair.

Unlike the classification described in Section 3.3.1, the photometric variables are continuous values and not discrete classes, and therefore require different analysis that can correlate the galaxy images with the continuous values. To weigh the numerical image content descriptors by their relevance to a specific photometric attribute, the Pearson correlation between each image feature f and the continuous variable v is used as described by Equation 3

$$W_f = \left| \frac{1}{N} \sum_{i=1}^N \left(\frac{f_i - \bar{f}}{\sigma_f} \right) \cdot \left(\frac{v_i - \bar{v}}{\sigma_v} \right) \right|, \quad (3)$$

where W_f is the weight assigned to feature f , and N is the number of images in the training set. After each image feature is assigned with a weight, the 85% of the features with the lowest weight are rejected from the analysis. The intuition of this weighting method is that numerical image content descriptors that have higher Pearson correlation with a certain photometry attribute better reflect the morphology that may be associated with it.

The predicted value of a given test image is determined by interpolating the

values of its five closest training samples, where the distance between a test image and training images is determined by the weighted Euclidean distance, such that the Pearson correlations are used as weights as described in Equation 4

$$d = \sqrt{\sum_{f=1}^{|X|} W_f (X_f - Y_f)^2}, \quad (4)$$

where W_f is the assigned Pearson correlation of feature f computed by Equation 3, and d is the computed weighted distance between the test feature vector X and a training feature vector Y . The method of correlating an image with a numerical variable is thoroughly described in (Shamir, 2011a), and the code is available (Shamir et al., 2013b).

The experiments were performed such that for each photometric variable 8,000 were selected randomly as a training set, and 2,000 were selected as test set. That was repeated 10 times for each photometric variable such that in each run different galaxies were selected randomly for training and test sets. The Pearson correlations between the value of the actual value of the variable and the predicted value based on the morphology of the galaxy was averaged. A higher correlation suggests that there is a stronger link between the value of the variable and the morphology of the galaxy. Table 3 shows the photometric variables with Pearson correlation higher than 0.1, all of these correlations are statistically significant.

Pearson Correlation	Variable
0.6592	u_r
0.6555	u_i
0.6383	q_i
0.6373	q_z
0.6355	q_r
0.6149	u_z
0.6117	u_g

0.5529	fracDeV_r
0.5348	fracDeV_i
0.5226	fracDeV_g
0.5203	q-g
0.5115	modelMag_u
0.5101	fracDeV_z
0.4978	expPhi_r
0.4964	expMag_u
0.4926	deVMag_u
0.489	deVPhi_g
0.4886	deVPhi_r
0.4847	petroMag_i
0.4838	expPhi_g
0.4817	expPhi_i
0.4803	expMag_i
0.4685	deVRad_r
0.4685	dere_d_u
0.4648	deVPhi_i
0.4625	deVMag_r
0.4609	expPhi_z
0.4594	z
0.4546	deVAB_i
0.4528	deVPhi_z
0.4528	dere_d_z
0.4519	r
0.4505	modelMag_g
0.4503	modelMag_z
0.45	deVMag_z
0.4493	deVAB_r
0.4483	deVRad_g

0.4477	fiberMag_r
0.4471	deVRad_i
0.4455	expAB_r
0.445	expMag_g
0.4436	u
0.4433	modelMag_i
0.4432	deVMag_i
0.4402	petroMag_r
0.4378	dered_r
0.4362	expMag_z
0.4359	deVAB_g
0.435	i
0.4346	expRad_z
0.4335	deVMag_g
0.4322	fiberMag_z
0.4318	lnLStar_r
0.4284	fiberMag_g
0.4278	petroMag_u
0.4265	expAB_g
0.4233	expAB_i
0.4218	petroR90_g
0.4213	petroMag_z
0.4212	fiberMag_i
0.4199	petroMag_g
0.418	petroR50_i
0.4169	modelMag_r
0.4134	deVABErr_r
0.4119	expMag_r
0.4088	deVRad_z
0.4083	lnLDeV_g

0.4081	fiberMag_u
0.4068	g
0.4023	dere_d_i
0.3979	expRad_g
0.3937	psfMag_g
0.3927	modelMagErr_r
0.3926	dere_d_g
0.3895	htmID
0.3877	deVAB_z
0.3856	expABErr_r
0.3848	psfMag_z
0.3808	expAB_z
0.3803	lnLStar_i
0.3798	deVMagErr_r
0.3795	fiberMagErr_r
0.3762	expRad_r
0.3761	lnLStar_g
0.376	expRad_i
0.3721	psfMag_u
0.3721	psfMag_i
0.3674	psfMag_r
0.3628	fracDeV_u
0.3563	lnLExp_z
0.3549	deVMagErr_i
0.3512	lnLDeV_r
0.3502	deVPhi_u
0.3495	lnLStar_z
0.3453	modelMagErr_g
0.3451	lnLExp_i
0.3326	deVABErr_z

0.3317	texture_z
0.3313	deVRadErr_z
0.3294	deVRadErr_r
0.3291	petroRad_g
0.3231	lnLExp_r
0.3209	lnLDeV_z
0.3186	texture_i
0.3163	expPhi_u
0.3145	expMagErr_z
0.31	deVMagErr_u
0.3096	petroR90_r
0.3034	mE1_r
0.3015	deVRad_u
0.2976	lnLExp_g
0.2949	expMagErr_u
0.2887	petroR50_g
0.2858	modelMagErr_z
0.2821	lnLStar_u
0.2806	modelMagErr_i
0.2799	petroR50_r
0.2731	lnLDeV_i
0.2691	deVRadErr_i
0.2658	mE1_g
0.2656	mE2_r
0.2652	colcErr_z
0.2603	expRadErr_z
0.2581	petroRad_r
0.2561	mRrCc_r
0.2559	expRadErr_r
0.2531	deVRadErr_g

0.2498	mE1PSF_r
0.2474	deVABErr_g
0.2444	petroRad_i
0.2334	u_u
0.233	mE2_i
0.2297	deVABErr_i
0.2279	mE1_i
0.2242	modelMagErr_u
0.2237	expAB_u
0.2165	fiberMagErr_i
0.2067	deVAB_u
0.2064	mE1PSF_g
0.2009	petroR90Err_u
0.1961	deVMagErr_z
0.1945	mE2PSF_r
0.1925	mRrCc_z
0.1924	nProf_g
0.1912	expRadErr_i
0.1809	mRrCcPSF_r
0.1798	isoPhiGrad_u
0.1794	expABErr_z
0.1784	lnLDeV_u
0.1782	petroR90Err_i
0.1777	lnLExp_u
0.176	petroR90_i
0.1743	mE2PSF_g
0.1742	mE1PSF_i
0.1742	mE2PSF_i
0.1712	mRrCcPSF_u
0.1708	mRrCcPSF_g

0.1705	mCr4_g
0.1701	psfMagErr_i
0.1684	nProf_i
0.1657	petroR50_z
0.1638	mE1PSF_z
0.1635	texture_g
0.1615	colcErr_r
0.1609	isoA_u
0.1608	mE1PSF_u
0.1566	isoRowcGrad_u
0.1564	mE2PSF_u
0.1562	mRrCcPSF_z
0.1554	mCr4_i
0.154	petroRad_z
0.154	petroRadErr_u
0.1529	isoColc_u
0.1528	mRrCcPSF_i
0.1527	petroR50Err_r
0.1527	isoRowc_u
0.1524	isoAGrad_u
0.1515	uErr_g
0.1489	petroR90Err_z
0.148	expMagErr_i
0.1478	uErr_i
0.1468	deVMagErr_g
0.1459	petroR90Err_g
0.1447	isoAErr_u
0.1398	isoPhi_u
0.1382	psfMagErr_r
0.1371	isoColcGrad_u

0.1361	deVRadErr_u
0.1345	texture_r
0.1324	isoBGrad_u
0.1302	isoColcErr_u
0.1295	mCr4PSF_g
0.1282	petroMagErr_r
0.1248	mE2_z
0.1241	mCr4_r
0.124	isoPhiErr_u
0.1237	mCr4PSF_r
0.1234	mRrCcErr_i
0.1225	uErr_r
0.1212	qErr_g
0.1203	psfMagErr_u
0.1178	mCr4PSF_z
0.1152	petroR50Err_i
0.1149	expRadErr_g
0.1134	q_u
0.1134	isoB_u
0.1086	expRad_u
0.1048	mCr4PSF_u
0.1047	nProf_u
0.1037	mCr4_z
0.1029	mE1_z
0.1018	mE2E2Err_g
0.1006	expABErr_g

Table 3: Variables with Pearson correlation between the actual and predicted values greater than 0.1.

As the table shows, the variables that had the strongest correlation with

the morphology of the galaxies is the Stokes Q and U parameters measured in the different bands. The “Stokes U” parameter is measured in SDSS by $U = \frac{a-b}{a+b} \sin(2\phi)$, where a is the major axis, b is the minor axis of the galaxy, and ϕ is the position angle (Abazajian et al., 2009). As can be expected, the different magnitude variables also show strong correlation with the morphological descriptors of the galaxies, as well as the position angle variables measured in the different bands. However, the magnitude error also exhibits correlation with the morphology of the images, showing that the error in measuring the magnitude depends on the morphology of the galaxies.

6. Conclusion

The increasing importance of autonomous sky surveys and large astronomical databases reinforces the development and application of methods for automatic analysis of astronomical data. Manual analysis of galaxy morphology using crowdsourcing has provided datasets of galaxy morphology that were useful for numerous studies. However, despite the success of these campaigns to recruit a high number of volunteers, these activities did not provide a complete analysis of all galaxies with visible morphology. For instance, the successful Galaxy Zoo 1 campaign (Lintott et al., 2011) provided a “superclean” dataset of less than $7 \cdot 10^5$ galaxies, which is far smaller than the number of SDSS galaxies with identifiable morphology, and smaller than automatically annotated catalogs of the same digital sky survey (Kuminski and Shamir, 2016). In the era of LSST, it is clear that full morphological analysis of the galaxies imaged by the future digital sky survey will require automation.

Since many digital sky surveys provide both photometry and image data, these data can be combined to perform a more informative automatic analysis. Here we showed that when using photometry data the performance of the analysis is comparable to analyzing the images directly, and combining morphological and photometric descriptors improves the performance of two pattern recognition tasks – classification and query-by-example. Nearly all experiments

performed in this study showed improved performance when using both morphological and photometric features, although in some of the cases the improvement was marginal.

While the common photometric measurements computed by digital sky surveys reflect information from the images, these pre-defined standard measurements might not be able to contain all possible information about the morphology of the galaxy. Therefore, additional information provided by applying machine vision methods can improve the automatic analysis tasks. The experiments show that the machine vision analysis adds substantial additional information to tasks such as query-by-example of peculiar galaxies, while making marginal contribution to other tasks such as supervised classification of galaxies annotated by their morphological types.

As automatic methods are already producing catalogs, the methods described in this paper can be used for tasks such as automatic annotation of galaxies to allow structured queries of the data, as well as query-by-example to identify collections of galaxies that are similar to a query galaxy.

The source code of the method is publicly available (Shamir, 2017) through the Astrophysics Source Code Library (Allen et al., 2012), or at <http://vfacstaff.ltu.edu/lshamir/downloads/UDAT>.

7. Acknowledgments

This study was supported by NSF grant IIS-1546079.

Funding for the SDSS and SDSS-II has been provided by the Alfred P. Sloan Foundation, the Participating Institutions, the National Science Foundation, the US Department of Energy, the National Aeronautics and Space Administration, the Japanese Monbukagakusho, the Max Planck Society, and the Higher Education Funding Council for England. The SDSS Web Site is <http://www.sdss.org/>. The SDSS is managed by the Astrophysical Research Consortium for the Participating Institutions. The Participating Institutions are the American Museum of Natural History, Astrophysical Institute Potsdam, University of Basel, Uni-

versity of Cambridge, Case Western Reserve University, University of Chicago, Drexel University, Fermilab, the Institute for Advanced Study, the Japan Participation Group, Johns Hopkins University, the Joint Institute for Nuclear Astrophysics, the Kavli Institute for Particle Astrophysics and Cosmology, the Korean Scientist Group, the Chinese Academy of Sciences (LAMOST), Los Alamos National Laboratory, the Max Planck Institute for Astronomy (MPIA), the Max Planck Institute for Astrophysics (MPA), New Mexico State University, Ohio State University, University of Pittsburgh, University of Portsmouth, Princeton University, the United States Naval Observatory and the University of Washington.

Appendix A. Using the code

To meet standard practices of using source code in academic literature (Shamir et al., 2013c), the source code developed and used in this study has been made available to the community through the Astrophysics Source Code Library (Allen et al., 2012, 2015). The code is also available at <http://vfacstaff.ltu.edu/lshamir/downloads/UDAT>. It can be compiled with GNU autotools, and binary files for MS-Windows are also available.

UDAT is a command line tool that can be used with a set of commands, as explained in (Shamir et al., 2008). In summary, testing the classification accuracy is done by the command:

```
udat test <switches> /path/to/dataset.fit /path/to/report.html
```

The file “dataset.fit” is the file of computed image numerical content descriptors and/or photometric descriptors, and it is also created by UDAT as will be described later in this section. The switches are explained in (Shamir et al., 2008), and a brief description is also available when typing “udat -h”. The file “report.html” is an optional file describing the results of the experiment, and it is created automatically by UDAT.

To classify a single galaxy the following command can be used:

```
udat classify <switches> /path/to/dataset.fit /path/to/image.tif
```

Note that the images should be in TIF or PPM format.

The query-by-example can be run in a similar fashion: `udat qbe <switches> /path/to/dataset.fit /path/to/query_image.tif`

By default, the command will only return the sample in the dataset that is the most similar to the query sample. To return more than one sample, the switch “N” can be used, followed by the number of samples that the query returns. For instance, using the switch “-N10” will return the 10 samples in the dataset that are determined by the algorithm to be the most similar to the query sample.

The step of computing the image numerical content descriptors for creating the dataset files (in the example above the file is called “dataset.fit”) is performed by the following command:

```
udat compute <switches> /path/to/input_file.cor /path/to/dataset.fit
```

The command will create the file “dataset.fit” from the information specified in the file “input_file.cor”. The file “input_file.cor” is a text file of the following format:

```
/path/to/image1.tif <tab> <class_id>,photometric_value1,photometric_value2,photometric_value3,...  
/path/to/image2.tif <tab> <class_id>,photometric_value1,photometric_value2,photometric_value3,...  
/path/to/image3.tif <tab> <class_id>,photometric_value1,photometric_value2,photometric_value3,...  
.  
.  
.
```

UDAT computes the morphological features from each image specified by the full path to an image file name, and then adds the photometric features values to the feature vector of each image to create the combined dataset of

morphological and photometric features.

It should be noted that the process of computing the numerical content descriptors is computationally intensive (Shamir et al., 2008) that normally requires a computing cluster (Shamir and Wallin, 2014; Kuminski and Shamir, 2016). The resulting output file can also be large, and each sample can add ~ 30 kilobyte to the size of the file.

References

- Abazajian, K.N., Adelman-McCarthy, J.K., Agueros, M.A., Allam, S.S., Prieto, C.A., An, D., Anderson, K.S., Anderson, S.F., Annis, J., Bahcall, N.A., et al., 2009. The seventh data release of the sloan digital sky survey. *The Astrophysical Journal Supplement Series* 182, 543.
- Abraham, R.G., Van Den Bergh, S., Nair, P., 2003. A new approach to galaxy morphology. i. analysis of the sloan digital sky survey early data release. *The Astrophysical Journal* 588, 218.
- Allen, A., Berriman, G.B., DuPrie, K., Mink, J., Nemiroff, R., Robitaille, T., Shamir, L., Shortridge, K., Taylor, M., Teuben, P., et al., 2015. Improving software citation and credit. arXiv preprint arXiv:1512.07919 .
- Allen, A., Teuben, P., Nemiroff, R.J., Shamir, L., 2012. Practices in code discoverability: Astrophysics source code library. arXiv preprint arXiv:1202.1028 .
- Almeida, J.S., Aguerri, J., Muñoz-Tuñón, C., De Vicente, A., 2010. Automatic unsupervised classification of all sloan digital sky survey data release 7 galaxy spectra. *The Astrophysical Journal* 714, 487.
- Arp, H.C., Madore, B., 1987. *A Catalogue of Southern Peculiar Galaxies and Associations: Volume 1, Positions and Descriptions.* volume 1. Cambridge University Press.

- Baillard, A., Bertin, E., de Lapparent, V., Fouqué, P., Arnouts, S., Mellier, Y., Pelló, R., Leborgne, J.F., Prugniel, P., Makarov, D., et al., 2011. The efigi catalogue of 4458 nearby galaxies with detailed morphology. *Astronomy & Astrophysics* 532, 74.
- Baillard, A., Bertin, E., Mellier, Y., McCracken, H., Géraud, T., Pelló, R., Leborgne, F., Fouqué, P., 2006. Project efigi: Automatic classification of galaxies, in: *Astronomical Data Analysis Software and Systems XV*, p. 236.
- Ball, N.M., Brunner, R.J., Myers, A.D., Tchong, D., 2006. Robust machine learning applied to astronomical data sets. i. star-galaxy classification of the sloan digital sky survey dr3 using decision trees. *The Astrophysical Journal* 650, 497.
- Ball, N.M., Loveday, J., Fukugita, M., Nakamura, O., Okamura, S., Brinkmann, J., Brunner, R.J., 2004. Galaxy types in the sloan digital sky survey using supervised artificial neural networks. *Monthly Notices of the Royal Astronomical Society* 348, 1038–1046.
- Banerji, M., Lahav, O., Lintott, C.J., Abdalla, F.B., Schawinski, K., Bamford, S.P., Andreescu, D., Murray, P., Raddick, M.J., Slosar, A., et al., 2010. Galaxy zoo: reproducing galaxy morphologies via machine learning. *Monthly Notices of the Royal Astronomical Society* 406, 342–353.
- Bishop, C.M., 2006. Pattern recognition. *Machine Learning* 128, 1–58.
- Borne, K., 2013. Virtual observatories, data mining, and astroinformatics, in: *Planets, Stars and Stellar Systems*. Springer, pp. 403–443.
- Calvi, R., Poggianti, B.M., Vulcani, B., 2011. The padova–millennium galaxy and group catalogue (pm2gc): the group-finding method and the pm2gc catalogues of group, binary and single field galaxies. *Monthly Notices of the Royal Astronomical Society* 416, 727–738.
- Davis, D.R., Hayes, W.B., 2014. Sparcfire: Scalable automated detection of spiral galaxy arm segments. *The Astrophysical Journal* 790, 87.

- De Vaucouleurs, G., De Vaucouleurs, A., Corwin Jr, H., Buta, R., Paturel, G., Fouque, P., 1992. Third reference catalogue of bright galaxies (rc3). VizieR Online Data Catalog 7137, 0.
- Dieleman, S., Willett, K.W., Dambre, J., 2015. Rotation-invariant convolutional neural networks for galaxy morphology prediction. *Monthly Notices of the Royal Astronomical Society* 450, 1441–1459.
- Djorgovski, S.G., Mahabal, A., Drake, A., Graham, M., Donalek, C., 2013. Sky surveys, in: *Planets, Stars and Stellar Systems*. Springer, pp. 223–281.
- Dojcsak, L., Shamir, L., 2014. Quantitative analysis of spirality in elliptical galaxies. *New Astronomy* 28, 1–8.
- Edwards, K.J., Gaber, M.M., 2014. *Astronomy and big data*. Springer.
- Hocking, A., Geach, J.E., Sun, Y., Davey, N., 2017. An automatic taxonomy of galaxy morphology using unsupervised machine learning. *Monthly Notices of the Royal Astronomical Society* 473, 1108–1129.
- Huertas-Company, M., Aguerri, J., Bernardi, M., Mei, S., Almeida, J.S., 2010. Revisiting the hubble sequence in the sdss dr7 spectroscopic sample: a publicly available bayesian automated classification. arXiv preprint arXiv:1010.3018 .
- Huertas-Company, M., Bernardi, M., Pérez-González, P., Ashby, M., Barro, G., Conselice, C., Daddi, E., Dekel, A., Dimauro, P., Faber, S., et al., 2016. Mass assembly and morphological transformations since $z \sim 3$ from candels. arXiv preprint arXiv:1606.04952 .
- Kuminski, E., George, J., Wallin, J., Shamir, L., 2014. Combining human and machine learning for morphological analysis of galaxy images. *Publications of the Astronomical Society of the Pacific* 126, 959–967.
- Kuminski, E., Shamir, L., 2016. A computer-generated visual morphology catalog of 3,000,000 sdss galaxies. *The Astrophysical Journal Supplement Series* 223, 20.

- Lekshmi, S., Revathy, K., Nayar, S.P., 2003. Galaxy classification using fractal signature. *Astronomy & Astrophysics* 405, 1163–1167.
- Lintott, C., Schawinski, K., Bamford, S., Slosar, A., Land, K., Thomas, D., Edmondson, E., Masters, K., Nichol, R.C., Raddick, M.J., et al., 2011. Galaxy zoo 1: data release of morphological classifications for nearly 900 000 galaxies. *Monthly Notices of the Royal Astronomical Society* 410, 166–178.
- Lupton, R., Blanton, M.R., Fekete, G., Hogg, D.W., OMullane, W., Szalay, A., Wherry, N., 2004. Preparing red-green-blue images from ccd data. *Publications of the Astronomical Society of the Pacific* 116, 133.
- Nair, P.B., Abraham, R.G., 2010. A catalog of detailed visual morphological classifications for 14,034 galaxies in the sloan digital sky survey. *The Astrophysical Journal Supplement Series* 186, 427.
- Orlov, N., Shamir, L., Macura, T., Johnston, J., Eckley, D.M., Goldberg, I.G., 2008. Wnd-charm: Multi-purpose image classification using compound image transforms. *Pattern Recognition Letters* 29, 1684–1693.
- Otsu, N., 1979. A threshold selection method from gray-level histograms. *IEEE Transactions on Systems, Man, and Cybernetics* 9, 62–66.
- Peng, C.Y., Ho, L.C., Impey, C.D., Rix, H.W., 2011. Galfit: Detailed structural decomposition of galaxy images. *Astrophysics Source Code Library* .
- Rubner, Y., Tomasi, C., Guibas, L.J., 2000. The earth mover’s distance as a metric for image retrieval. *International Journal of Computer Vision* 40, 99–121.
- Schutter, A., Shamir, L., 2015. Galaxy morphology an unsupervised machine learning approach. *Astronomy and Computing* 12, 60–66.
- Shamir, L., 2009. Automatic morphological classification of galaxy images. *Monthly Notices of the Royal Astronomical Society* 399, 1367–1372.

- Shamir, L., 2011a. A computer analysis method for correlating knee x-rays with continuous indicators. *International Journal of Computer Assisted Radiology and Surgery* 6, 699–704.
- Shamir, L., 2011b. Ganalyzer: A tool for automatic galaxy image analysis. *The Astrophysical Journal* 736, 141.
- Shamir, L., 2016. Morphology-based query for galaxy image databases. *Publications of the Astronomical Society of the Pacific* 129, 024003.
- Shamir, L., 2017. Udat: A multi-purpose data analysis tool. *Astrophysics Source Code Library* , ascl:1704.002.
- Shamir, L., Holincheck, A., Wallin, J., 2013a. Automatic quantitative morphological analysis of interacting galaxies. *Astronomy and Computing* 2, 67–73.
- Shamir, L., Ling, S.M., Scott Jr, W.W., Bos, A., Orlov, N., Macura, T.J., Eckley, D.M., Ferrucci, L., Goldberg, I.G., 2009. Knee x-ray image analysis method for automated detection of osteoarthritis. *IEEE Transactions on Biomedical Engineering* 56, 407–415.
- Shamir, L., Orlov, N., Eckley, D.M., Macura, T., Johnston, J., Goldberg, I., 2013b. Wnd-charm: Multi-purpose image classifier. *Astrophysics Source Code Library* , ascl:1312.002.
- Shamir, L., Orlov, N., Eckley, D.M., Macura, T., Johnston, J., Goldberg, I.G., 2008. Wndchrn—an open source utility for biological image analysis. *Source Code for Biology and Medicine* 3, 13.
- Shamir, L., Wallin, J., 2014. Automatic detection and quantitative assessment of peculiar galaxy pairs in sloan digital sky survey. *Monthly Notices of the Royal Astronomical Society* 443, 3528–3537.
- Shamir, L., Wallin, J.F., Allen, A., Berriman, B., Teuben, P., Nemiroff, R.J., Mink, J., Hanisch, R.J., DuPrie, K., 2013c. Practices in source code sharing in astrophysics. *Astronomy and Computing* 1, 54–58.

- Shamir, L., Yerby, C., Simpson, R., von Benda-Beckmann, A.M., Tyack, P., Samarra, F., Miller, P., Wallin, J., 2014. Classification of large acoustic datasets using machine learning and crowdsourcing: Application to whale calls. *The Journal of the Acoustical Society of America* 135, 953–962.
- Simard, L., 1998. Gim2d: an iraf package for the quantitative morphology analysis of distant galaxies, in: *Astronomical Data Analysis Software and Systems VII*, p. 108.
- Timmis, I., Shamir, L., 2017. A catalog of automatically detected ring galaxy candidates in panstarss. *The Astrophysical Journal Supplement Series* 231, 2. URL: <http://stacks.iop.org/0067-0049/231/i=1/a=2>.
- Vasconcellos, E., De Carvalho, R., Gal, R., LaBarbera, F., Capelato, H., Velho, H.F.C., Trevisan, M., Ruiz, R., 2011. Decision tree classifiers for star/galaxy separation. *The Astronomical Journal* 141, 189.
- Willett, K.W., Lintott, C.J., Bamford, S.P., Masters, K.L., Simmons, B.D., Casteels, K.R., Edmondson, E.M., Fortson, L.F., Kaviraj, S., Keel, W.C., et al., 2013. Galaxy zoo 2: detailed morphological classifications for 304 122 galaxies from the sloan digital sky survey. *Monthly Notices of the Royal Astronomical Society* , stt1458.

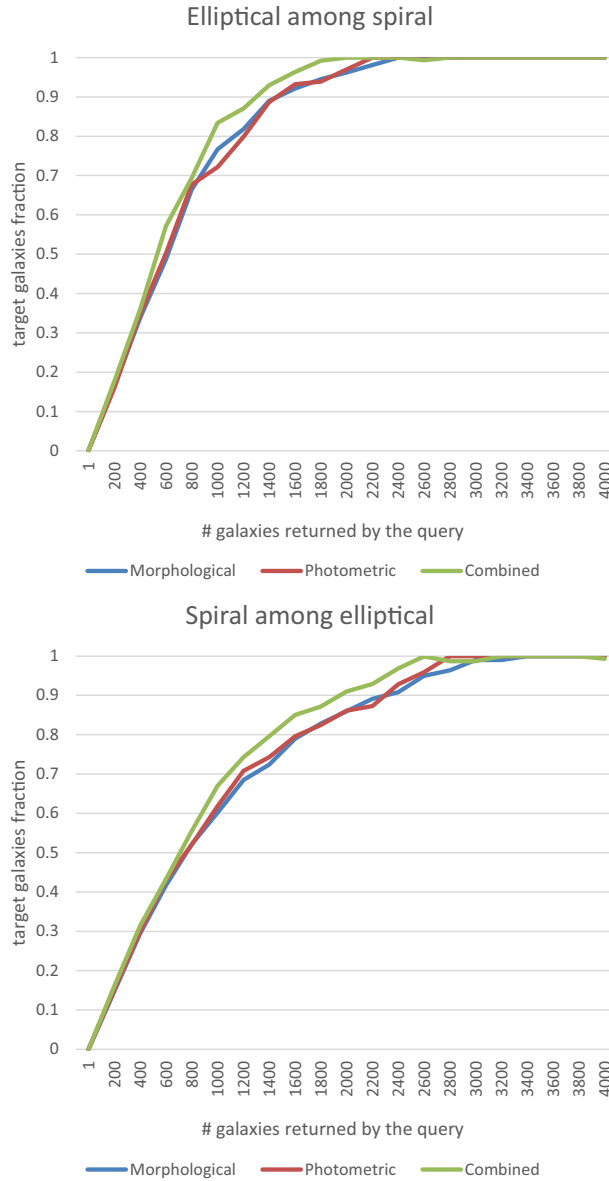


Figure 10: The portion of elliptical galaxies (top) and spiral galaxies (bottom) when combining 1,000 target galaxies with 4,000 database galaxies. The Y axis shows the number of the target galaxies (elliptical or spiral) returned by the algorithm divided by the total number of target galaxies.

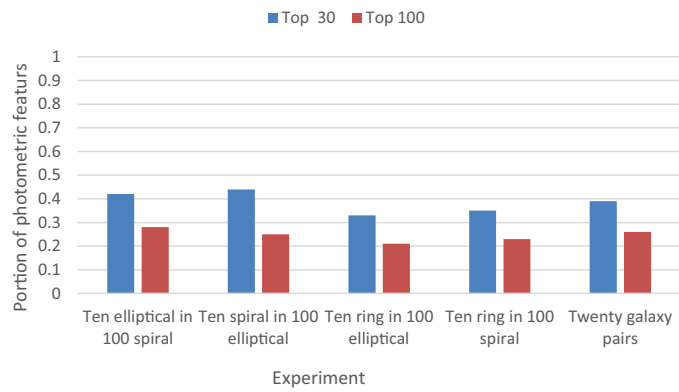


Figure 11: Distribution of the photometric and morphological features in each of the experiments.